Patient-specific image segmentation and adaptive mesh generation

Alexander A. Danilov[1,2], Roman A. Pryamonosov[1], Alexandra S. Yurova[1,3]

[1]Institute of Numerical Mathematics, Russian Academy of Sciences, Moscow, Russia
[2]Moscow Institute of Physics and Technology, Dolgoprudny, Russia
[3]Lomonosov Moscow State University, Moscow, Russia

Introduction

We develop and present methods and algorithms for patient-specific image segmentation and generation of discrete geometric models for several medical applications. We consider two types of modelling applications: applications requiring individualized regional network of blood vessels, e.g. haemodynamics modelling; and applications requiring the full torso tissues structure, e.g. bioimpedence analysis or electrocardiography (ECG) modelling.

Vascular network reconstruction consists of several stages (Fig. 1). We focus on coronary and cerebral arteries segmentation.

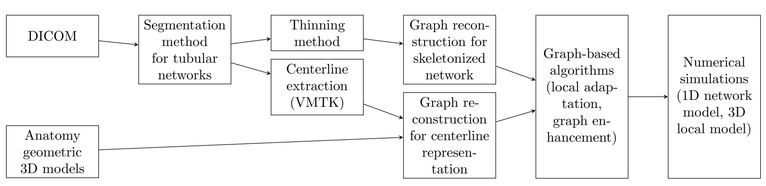

Figure 1: Admissible flowcharts of vascular network reconstruction algorithms.

Coronary arteries segmentation

Contrast enhanced Computed Tomography Angiography (ceCTA) DICOM images are used as input data. Our automatic vessel segmentation methodology for coronary arteries was proposed in [1]. Essential steps of this method consist of aorta segmentation (Fig. 2), computation of vesselness values, searching branches of aorta arch or ostia points, and removing segmentation errors near aorta boundary.

We employ the Isoperimetric Distance Trees (IDT) [2] algorithm for aorta segmentation. It starts from the mask M_{init} and a voxel c, it cuts the mask M_{init} through bottlenecks and outputs submask M_A containing c. The Circle Hough Transform [3] is used to detect an aorta cross-section – the largest bright disk D and its radius R_A on transverse planes (Fig. 2a). Initial mask is acquired by thresholding method with a minimal intensity inside of the disk t_{init} as a threshold parameter (Fig. 2b). The center of the disk is considered as the initial voxel c.

After the IDT stage, some parts of coronary arteries may still be included in M_A (Fig. 2c). We define mask *smoothing* with parameter p as successive deletion of p voxels thick border from the mask (p-*border*) and addition of p-border. High smoothing parameter values result in mask distortion. In the coronary case a simple morphological smoothing of M_A with small parameter is sufficient in order to remove coronary parts and to keep the mask intact (Fig. 2d-e).

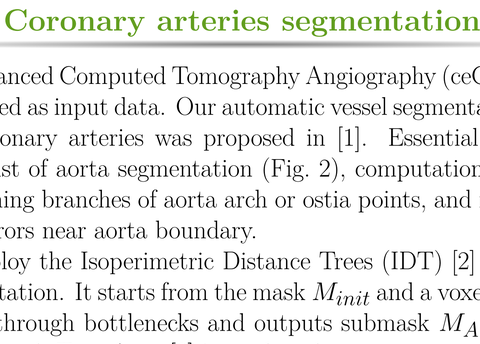

Figure 2: Flowchart for automatic segmentation of aorta.

The next step is computation of Frangi Vesselness [4], which results in bigger values inside bright tubular structures. Segmentation of arteries is produced by thresholding of vesselness values. Then coronary arteries and cerebral aorta arch branches are found as voxel connectivity components near the aorta boundary.

Cerebral arteries segmentation

Bone elimination is an essential step for cerebral artery segmentation due to vertebral arteries and cervical vertebrae proximity. Assuming both CT and ceCTA datasets (Fig. 3a-b) are available for the same patient, bones can be automatically darkened with the multiscale matched mask bone elimination algorithm [5] (Fig. 3c). Aortic arch branches are defined as connected components of voxels with high vesselness, lying close to aorta border (Fig. 3d-f). Aorta border cleaning is the final step, which is necessary since high vesselness values may falsely occur near big bright structures (Fig. 3g).

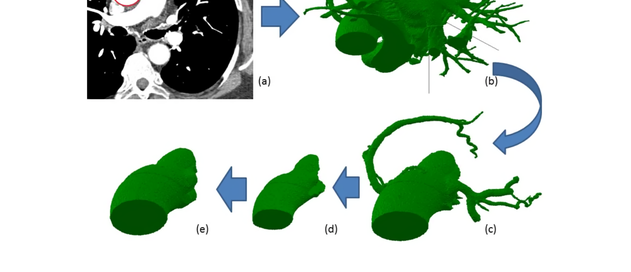

Figure 3: Flowchart for automatic segmentation of cerebral arteries.

We assume the mask M_V represents the vessels, and the mask M_A represents only the aorta. We define the voxel layer $L_d = \{v \in M_V \mid dist(M_A, v) = d\}$ as a subset of mask M_V distanced from the mask M_A by the distance d. For each voxel layer L_d for $d = d_{\max}, \ldots, 0$ we apply the following procedure: remove all voxels from L_d that have no adjacent voxels in L_{d+1}. The parameter $d_{\max}$ should be big enough, so that voxel layer $L_{d_{\max}}$ contains no segmentation errors.

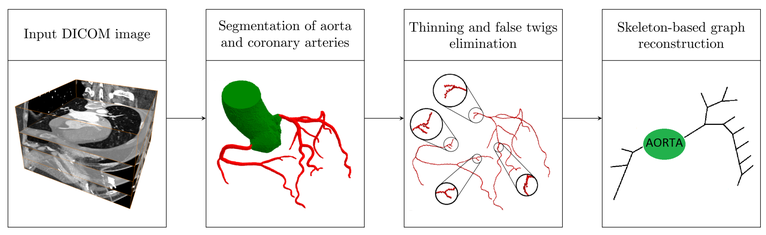

Figure 4: Flowchart for automatic reconstruction of coronary arteries 1D network.

Vascular network reconstruction

We adopt the Distance-Ordered Homotopic Thinning proposed by C. Pudney [6] for skeletonization. The algorithm starts with a binary image and outputs the topologically equivalent skeleton centered with respect to the shape of the image. The centredness of the skeleton is determined by the order of voxel elimination from the image. Following [6], we use a chamfer distance transform approximating Euclidean distance.

During the thinning process the voxels are sorted by distance values in ascending order and are deleted in groups with the equal values. A voxel is deletable if it is simple and not the end of a medial axis (i.e. it is adjacent to one and only one voxel). In practice this approach leads to a skeleton with several false twigs, usually near bifurcations and flattened vessels, which do not correspond to any actual vessel. False twigs are attributed to superfluous topology features caused by initial image noises and irregularities of vessel shape. We apply a post-processing stage to eliminate false twigs: all segments with length smaller than the local vessel radius are eliminated (Fig. 4).

Results of automatic segmentation, skeletonization, and network reconstruction for two coronary datasets (CD1, CD2), two cerebral datasets (ND1, ND2), and a vascular corrosion cast of rabbit kidney (RK) are presented in Figs. 5–7. CPU times of specific segmentation and skeletonization stages are presented in Tables 1–3.

Experiment with RK dataset shows good efficiency and robustness of the skeletonization algorithm.

Figure 5: Segmentation and skeletonization for coronary datasets CD1 (left), CD2 (right).

Table 1: Dataset resolution and CPU time of coronary segmentation stages.

Dataset	CD1	CD2
Resolution	$512 \times 512 \times 248$	$512 \times 512 \times 211$
Spacing	$0.37 \times 0.37 \times 0.40$ mm	$0.46 \times 0.46 \times 0.48$ mm
Aorta segmentation	5.80 s	5.19 s
Frangi filter	91.76 s	73.94 s

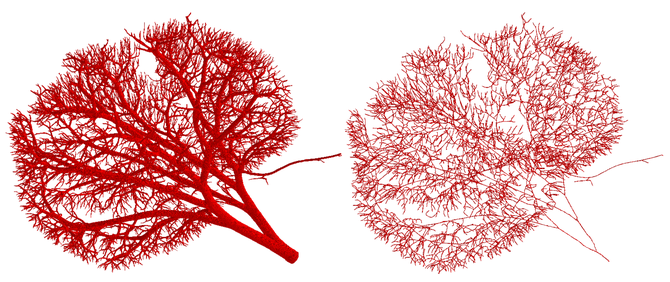

Figure 6: Reconstruction of rabbit kidney vascular network (RK). μCT DICOM data provided by J. Alastruey [7, 8].

Table 2: CPU time of skeletonization and graph reconstruction stages.

Dataset	CD1	RK
Resolution	$512 \times 512 \times 248$	$2000 \times 1989 \times 910$
Distance map	0.20 s	58.12 s
Thinning	0.79 s	526.98 s
False twigs elimination	0.15 s	16.61 s
Graph construction	0.13 s	12.27 s
Skeletal segments	22	4302
False twigs	6	2142

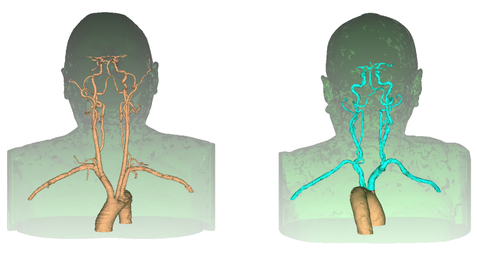

Figure 7: Cerebral arteries segmentation for datasets ND1 (left) and ND2 (right).

Table 3: CPU times of cerebral arteries segmentation.

Dataset	ND1	ND2
Resolution	$512 \times 512 \times 501$	$512 \times 512 \times 451$
Spacing	$0.76 \times 0.76 \times 0.80$ mm	$0.62 \times 0.62 \times 0.80$ mm
Pulmonary removal	7.76 s	7.04 s
Aorta segmentation	16.61 s	15.33 s
Frangi vesselness	196.40 s	184.91 s
Aortic arch branches	7.61 s	6.67 s
Aorta border cleaning	7.39 s	6.76 s

Adaptive mesh generation

Several techniques for soft tissue segmentation are used, including user-guided active contour segmentation with supervised random forest classification and textural features computation [9, 10, 11].

An example of human heart segmentation is presented in Fig. 8. The adaptive unstructured tetrahedral mesh was constructed using Delaunay triangulation algorithm from CGAL Mesh library [12]. The maximum mesh size is 3 mm, the minimum mesh size in the vicinity of heart boundaries and material interfaces is 1 mm. The computational mesh consists of 367 318 tetrahedra and 77 953 vertices. Upscaling of multi-labeled segmented image was used to improve the resolution of input data.

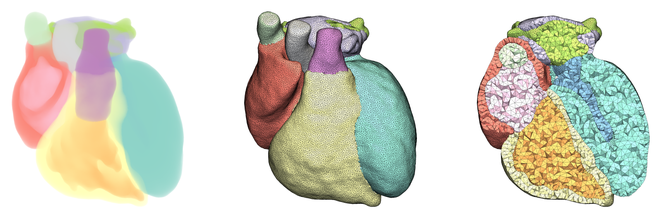

Figure 8: Unstructured mesh for human heart: translucent 3D model, triangular surface mesh, and volume cut of the tetrahedral mesh.

Adaptive mesh size may be used to improve mesh resolution in the region of interest while keeping the total number of mesh elements reasonable. Fig. 9 demonstrates the results of forward ECG calculation using adaptive unstructured mesh for Visible Human Project (VHP) data.

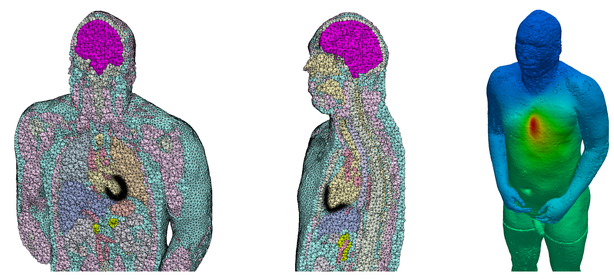

Figure 9: VHP male body mesh refined near heart ventricles and body surface electrical potential calculated during ECG modelling.

Conclusion

The work addresses several segmentation techniques for generation of individualized computational domains from medical imaging datasets. We propose automatic algorithms for vascular network segmentation. We present several examples of patient-specific segmentation and skeletonization. We discuss soft tissue segmentation and adaptive mesh generation. The proposed algorithms are presented in details in our works [1, 9, 10, 11].

Acknowledgements

The work was supported by the Russian Science Foundation (RSF) grant 14-31-00024.

References

[1] A. Danilov, Y. Ivanov, R. Pryamonosov, and Y. Vassilevski. Methods of graph network reconstruction in personalized medicine. *International Journal for Numerical Methods in Biomedical Engineering*, 32:e02754, 2016.

[2] L. Grady. Fast, quality, segmentation of large volumes – Isoperimetric distance trees. *Computer Vision – ECCV 2006*, 3953:449–462, 2006.

[3] R. O. Duda and P. E. Hart. Use of the Hough transformation to detect lines and curves in pictures. *Communications of the ACM*, 15:11–15, 1972.

[4] A. Frangi, W. Niessen, K. Vincken, and M. Viergever. Multiscale vessel enhancement filtering. In *Medical Image Computing and Computer-Assisted Intervention – MICCAI'98*, 130–137, 1998.

[5] H. A. F. G. van Andel, H. W. Venema, G. J. Streekstra, et al. Removal of bone in CT angiography by multiscale matched mask bone elimination. *Medical Physics*, 34:449–462, 2007.

[6] C. Pudney. Distance-ordered homotopic thinning: A skeletonization algorithm for 3D digital images. *Computer Vision and Image Understanding*, 72:404–413, 1998.

[7] J. Alastruey, S. R. Nagel, B. A. Nier, et al. Modelling pulse wave propagation in the rabbit systemic circulation to assess the effects of altered nitric oxide synthesis. *Journal of Biomechanics*, 42:2116–2123, 2009.

[8] J. Alastruey, A. A. E. Hunt, and P. D. Weinberg. Novel wave intensity analysis of arterial pulse wave propagation accounting for peripheral reflections. *International Journal for Numerical Methods in Biomedical Engineering*, 30:249–279, 2013.

[9] A. A. Danilov, R. A. Pryamonosov, and A. S. Yurova. Image segmentation techniques for biomedical modeling: electrophysiology and hemodynamics. In *Proceedings of the 7th European Congress on Computational Methods in Applied Sciences and Engineering (ECCOMAS 2016)*, 2016.

[10] Y. V. Vassilevski, A. A. Danilov, S. S. Simakov, et al. Patient-specific anatomical models in human physiology. *Russian Journal of Numerical Analysis and Mathematical Modelling*, 30:185–201, 2015.

[11] A. Danilov, R. Pryamonosov, and A. Yurova. Image segmentation for cardiovascular biomedical applications at different scales. *Computation*, 4:35, 2016.

[12] L. Rineau, M. Yvinec. A generic software design for Delaunay refinement meshing. *Computational Geometry*, 72:100–110, 2007.

Contact Information

- Alexander A. Danilov
- e-mail: a.a.danilov@gmail.com

Supplementary materials are available online:
http://dodo.inm.ras.ru/danilov/vph-2016/